

APPLICATIONS OF STEREOLOGY IN MATERIALS SCIENCE AND ENGINEERING

Arun M. Gokhale and Nishkamraj U. Deshpande

School of Materials Science and Engineering
Georgia Institute of Technology
Atlanta, Georgia - 30332-0245, U.S.A.

ABSTRACT

There has been significant progress in theoretical stereology during past decade or so. The practical applications of stereology (at least in materials science) have not kept pace with the rapid theoretical advance: stereological measurements other than volume fraction and grain size are rarely used in materials science, although microstructure - properties - processing studies are of central importance! It is the purpose of this presentation to discuss some applications of stereology for the study of materials processes, where quantification of microstructure and its evolution has lead to useful information.

Keywords: microcracks, sintering, fractography, metal matrix composites, recrystallization, Aluminum alloys, creep fracture.

INTRODUCTION

There have been very significant advances in theoretical stereology during the past decade. The basic attributes of the microstructural features, namely, total volume, surface area, length, number, and connectivity can be now estimated efficiently. Volume fraction is accessible via point counting (see Underwood, 1970), or ribbon probe (McMillan, 1992), surface area can be estimated from the vertical sections (Baddeley, Gundersen, and Cruz-Orive, 1986), length density can be estimated efficiently from the vertical slices (Gokhale, 1990, 1992, 1993), absolute feature length can be estimated from vertical projections (Cruz-Orive and Howard, 1991), and number and connectivity can be measured from the dissector and related 3D probes (Sterio, 1984, Cruz-Orive, 1987, DeHoff, 1987, Gundersen, 1988). These developments have helped to transform stereology into a practical, versatile, and useful tool for the characterization of microstructures. The progress in second order stereology enables characterization of the spatial distribution of the microstructural features (Stoyan, 1985, Cruz-Orive, 1989, Jensen, Kieu and Gundersen, 1990). Application of stereology for characterization of fracture surfaces has yielded general, assumption-free techniques for estimation of fracture surface roughness from the vertical section fracture profiles (Gokhale and Underwood, 1990, Gokhale and Drury, 1990, 1993); the attributes such as fractal dimension can be also estimated from 2D sections (Mandelbrot, 1983, Drury and

Gokhale, 1993). The advances in mathematical morphology (Serra, 1988, Meyer, 1992) have provided rigorous techniques for automatic and interactive image analysis. The practical applications of stereology and image analysis (at least in materials science) have not kept the pace with the rapid theoretical advance: the stereological measurements other than grain size and volume fraction are not used very frequently for the characterization of materials microstructures. However, when stereology is correctly applied to study the materials processes, it has often lead to new insights and quantitative information regarding the materials processes. The applications of stereology and image analysis in materials science can be grouped into the following broad categories.

(1) Quantitative characterization of microstructural evolution during the processes such as phase transformations, sintering, deformation, damage evolution in composites, etc. to obtain the basic information regarding the processes that lead to the changes in the microstructure.

(2) Application of stereology for the characterization of nonplanar and geometrically complex fracture surfaces, i.e., quantitative fractography.

(3) Development of quantitative microstructure-properties correlations.

It is the purpose of this paper to present applications of stereology to illustrate how stereology and image analysis can be utilized to obtain useful information regarding the behavior of materials. The next section of the paper deals with the applications in the areas of damage evolution in composites during thermal cycling, and of estimation of the growth rates of "necks" during sintering of iron powder. Applications to the study of fracture (fractography) are presented in the subsequent section.

MICROSTRUCTURAL EVOLUTION

Materials processes such as phase transformations, sintering, deformation, creep, fatigue, thermal cycling, etc. lead to changes in the microstructure. The microstructural evolution is basically due to the motion of microstructural interfaces, lines, and points (i.e., growth or shrinkage), and/or changes in the number of microstructural features due to formation (nucleation) of new features or annihilation of existing features, as a function of the extent of the process. In such cases, the kinetic informations of fundamental importance are growth rates of microstructural features (or more precisely, distribution of interface and/or edge velocities, etc.), and rates of nucleation or annihilation of the microstructural features of interest. These "rates" are not necessarily time derivatives; the rates may be with respect to strain (for example, microvoid growth during deformation), or number of cycles (as in fatigue or thermal cycling), or any other independent variable that induces changes in the microstructure. The evolution processes can be studied by estimating the metric and/or topological properties of interest at different times (or at different number of cycles, etc.) during the process. The microstructural properties data can be utilized to extract the nucleation and growth information (see Gokhale and DeHoff, 1985, DeHoff, 1986, Gokhale, 1992, Vandermeer, 1992). The procedure is illustrated via the following two examples, where the evolution processes are relatively simple.

Thermal Cycling of Metal Matrix Composite

Figure 1 shows micrograph of metal matrix composite (MMC) having continuous, aligned alumina fibers in the matrix of Al-2.5% Li alloy (the sectioning plane is perpendicular to the fibers). There is a large difference between the thermal expansion coefficient of the fibers and

the matrix (more than a factor of five). Due to this thermal mismatch, the thermal cycling leads to cyclic thermal stresses that result in the formation and growth of microcracks in the composite. Figure 2 shows micrograph of a specimen after 3000 thermal cycles in the temperature range of room temperature to 325°C. The microcracks are observed between the fiber pairs. It is of significant practical interest to study the formation and growth of such thermally induced microcracks, and to correlate the temperature cycle parameters and the microstructure of the MMC to the formation and growth rates of the microcracks.

A microcrack consists of two surfaces bound by an edge. Each microcrack has volume, surface area, and Euler characteristics associated with it. The growth of the microcrack increases its volume and surface area. Thus, estimation of the volume fraction V_v , total surface area per unit volume S_v , and the number density of microcracks as function of the number of thermal cycles n , should provide quantitative information on the nucleation and growth of the microcracks.

Gokhale and Whited (1992) monitored the microcrack evolution by estimating the V_v and S_v of the microcracks and the number of microcracks per unit area in the plane perpendicular to the fiber axis, N_A , in a series of specimens thermally cycled between 10 to 5000 cycles (experimental details are given in Whited, 1992). The volume fraction was estimated by point counting. The total microcrack surface area was estimated by using the concept of vertical sections (Baddeley, et al., 1986). The direction perpendicular to the plane of the specimen plate was chosen as vertical axis, and S_v was estimated from three vertical sections mutually at an angle of 120° by using oriented cycloid test lines. It is shown that such a composite test probe (called "trisector") yields efficient and precise estimate of S_v from just three vertical sections irrespective of the nature of anisotropy (Drury and Gokhale, 1993). Figure 3 shows a plot of the ratio of the number of microcracks per unit area N_A to the number of fibers per unit area N_f in the plane perpendicular to the fibers versus the number of thermal cycles, n , experienced by the specimen. It is interesting to note that N_A/N_f does not vary significantly with the number of thermal cycles. From simple geometric considerations, it can be shown that,

$$N_A/N_f = N_v \cdot \bar{L}/N_f \quad (1)$$

where N_v is the number of microcracks per unit volume, and \bar{L} is the average microcrack length in the direction parallel to the fibers. Since, the fiber density N_f can not depend on thermal cycles, and N_A/N_f is constant, it follows that: (i) the number of microcracks per unit volume, N_v , does not increase with the number of thermal cycles, and hence most of the microcracks are formed at very early stages of the process, and (ii) the microcracks reach saturation length in the direction parallel to the fibers, soon after they are formed, and this dimension does not increase significantly with the subsequent thermal cycles. For such a microcrack growth geometry it can be shown that the ratio of S_v/N_A directly gives the average value of the microcrack dimension that does increase due to the thermal cycling (Whited, 1992, Gokhale and Whited, 1992). Figure 4 shows the plot of S_v/N_A versus the number of thermal cycles n . The slope of the plot gives the microcrack growth rate; the data shows that the microcracks grow at an approximately constant rate of 5×10^{-5} mm/sec for the thermal cycle studied. It is interesting to note that unlike the fatigue cracks driven by the cyclic mechanical stresses, the thermally induced microcracks do not grow faster as their size increases! The quantitative data on microcrack growth are useful for developing and verifying analytical and computer models for damage evolution, and for correlating the composite microstructure to the damage and its evolution. The

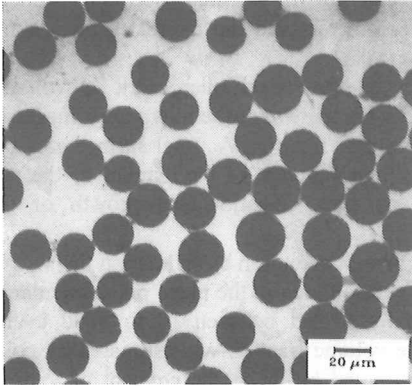


Fig. 1. A micrograph of the as received MMC.

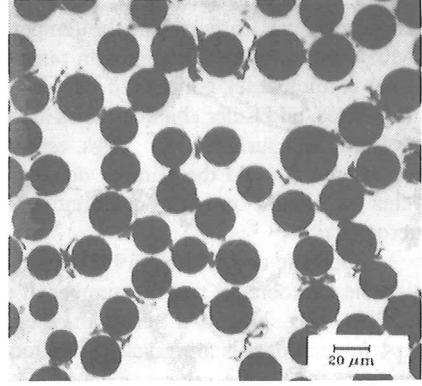


Fig. 2. A micrograph of the MMC after 3000 cycles.

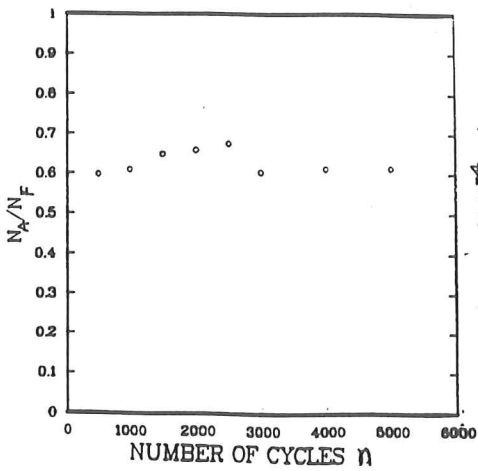


Fig. 3. Plot of N_A/N_F versus number of thermal cycles n

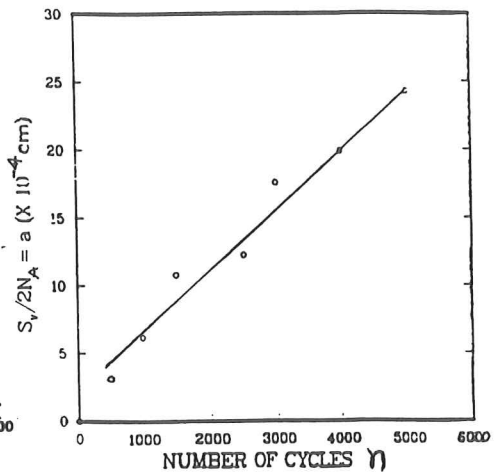


Fig. 4. Plot of S_v/N_A versus number of thermal cycles n

present technique can be also applied to microcrack growth during mechanical fatigue.

Sintering of Iron Powder

Sintering is a technologically important materials processing technique where a bulk component is produced from powder by compacting the powder and keeping it at high temperature (with or without applied stress or pressure) for sufficiently long time. During sintering, "necks" are developed between the powder particles that are in contact (see Figure 5); the neck size increases and the total area of solid/pore interfaces decreases with time. During sintering, the mass transport can occur via a number of different mechanisms. The theoretical models for sintering assume a rate controlling mechanism(s) and predict the growth law for the necks. It is of interest to test these models to determine their applicability in the system of interest.

Gokhale, Basavaiah, and Upadhyaya (1988) conducted a detailed stereological study of the evolution of necks during sintering of spherical iron powder of close size range (62 to 74 μm diameter) to verify the theoretical models for neck growth. A series of specimens were loose stack sintered for different times ranging from 0 to 34 hours at 950, 1000, and 1050°C in either dry hydrogen or argon atmosphere. A neck is a SSP (solid-solid-pore) triple line of contact between two powder particles and pore space (see Figure 6).

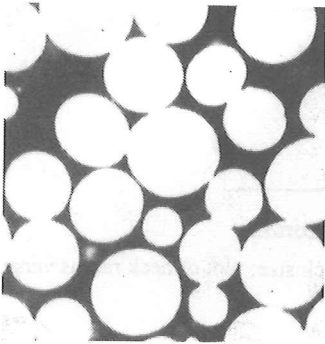


Fig.5. Micrograph of sintered Fe powder at 1050 °C for 24 hours (156X)

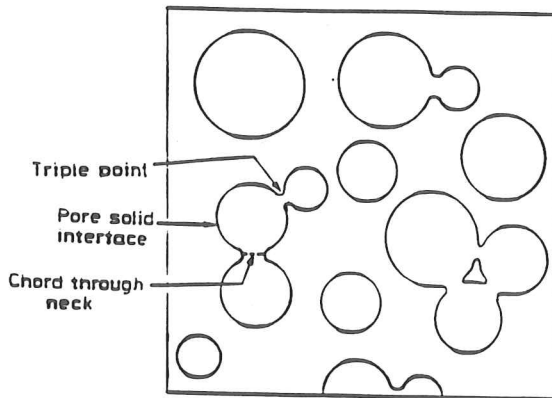


Fig. 6. Schematic showing SSP lines in the sintered metal

Since the powder particles are of spherical shape and approximately monosized, the necks (SSP triple lines) are expected to be of circular shape, and they are isotropically oriented. Intersections of these circular necks with a metallographic plane yield chords of different sizes; the distribution of these chord lengths was monitored as a function of sintering time. The total neck length per unit volume L_v was also calculated from the same data. The data analysis yielded the total number of necks per unit volume and hence number of interparticle contacts per particle, and the neck size X as a function of time. Figure-7 shows the time dependence of the calculated neck size X ; the solid curves show the growth kinetics predicted by different theoretical models.

It was observed that the number of interparticle contacts per particle does not change significantly with time and hence almost all the necks form in the initial stages of the sintering process; their number is basically determined by the initial stacking of the particles in the powder mass. The models for surface and grain boundary diffusion controlled sintering predict neck sizes and growth rates that are significantly higher than observed values. The surface, grain boundary, and volume diffusion are "parallel" diffusion paths, and hence the fastest should control the kinetics. Figure-7, however, shows that although, surface and grain boundary diffusion models predict much higher neck sizes (and hence the kinetics), the experimental data shows much slower growth kinetics than that predicted by these models! It must be then concluded that these models are not applicable due to the assumptions other than the rate controlling step: it is likely that the simplifying assumptions regarding neck geometry, intrinsic to these models, are not applicable.

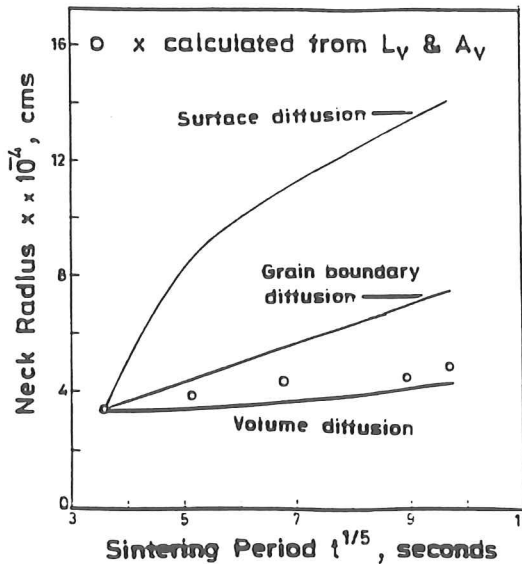


Fig. 7. Comparison of experimental and theoretical values of neck size; plot of neck radius versus $t^{1/5}$ at 950 °C

CHARACTERIZATION OF FRACTURE SURFACES

The end point of deformation and fracture processes is the generation of fracture surface. The fracture surfaces are usually nonplanar rough surfaces having complex geometry. The topography of a fracture surface and its microstructural features may contain information regarding the fracture mechanisms, and of the role of microstructural features in the fracture processes. The geometric attributes of fracture surface can be grouped in the following categories

- (1) Descriptors of global topography of fracture surface, such as roughness, fractal dimension, anisotropy, etc.
- (2) Feature specific properties such as asperity heights, dimple sizes, extent of overlaps, etc.
- (3) Geometric attributes of the microstructural features on the fracture surface. For

example, area fraction and number density of inclusions on the fracture surface.

The fracture surfaces are usually observed by SEM fractography, which gives a plane projection of a nonplanar surface. Fracture profiles generated by intersection(s) of fracture surface with metallographic plane, also provide information regarding fracture surfaces. This technique is called profilometry. Thus, stereology is necessary to estimate the attributes of fracture surface from either SEM or profilometric observations.

The fracture surface roughness parameter R_s (which is the ratio of true area of fracture surface to its projected area) can be estimated from the measurements performed on the vertical section fracture profiles by using the following assumption-free stereological relationship (Gokhale and Underwood, 1990).

$$R_s = \overline{R_L} \cdot \Psi \quad (1)$$

Ψ = Profile structure factor

where,

$$\Psi = \int_0^{\pi} [\sin \alpha + (\frac{\pi}{2} - \alpha) \cos \alpha] f(\alpha) d\alpha \quad (2)$$

R_L is the profile roughness parameter of a vertical section fracture profile (see Figure 8) and α is the angle between the tangent to the fracture profile at a given point and the vertical axis, $f(\alpha)$ is the frequency function of these orientation angles. The "bar" in equation (1) signifies averaging over vertical sections. The roughness measurements are useful for estimation of fractal dimension (Drury and Gokhale, 1993), and for calculating the parameters such as number density of microstructural features on the fracture surface (Antolovich et al., 1990). The derivation of equation (2) draws significantly from Baddeley's concept of sampling on vertical sections. Both R_L and $f(\alpha)$ can be estimated from the digitized fracture profile data; the procedure is described elsewhere (Banerji, 1988, Gokhale and Drury, 1990, 1993).

The estimation of feature specific properties (except dimple sizes) has not received much attention in the past. Recently, Gokhale and Drury (1993) have developed an algorithm to calculate the average asperity height and the height distribution directly from the digitized fracture profile data. This procedure has been applied to study crack closure during fatigue crack growth in Inconel-718 superalloy (Drury, 1992). The fraction of fracture profile length that is reentrant or overlapped can be also estimated directly from the digitized profile data. Mishra (1992) has utilized this procedure to study the creep fracture surfaces. Some practical applications of stereology for characterization of fracture surfaces are discussed below.

Effect of Recrystallization on Fracture Path of Aluminum Alloy

Wrought aluminum alloy 7050 is quite popular for structural applications. The alloy fabrication often involves hot rolling which results in the presence of recrystallized regions in the processed material. The fracture surface of the hot rolled 7050 alloy often contains intergranular (brittle) regions, and dimpled transgranular (ductile) regions. The fracture behavior depends significantly

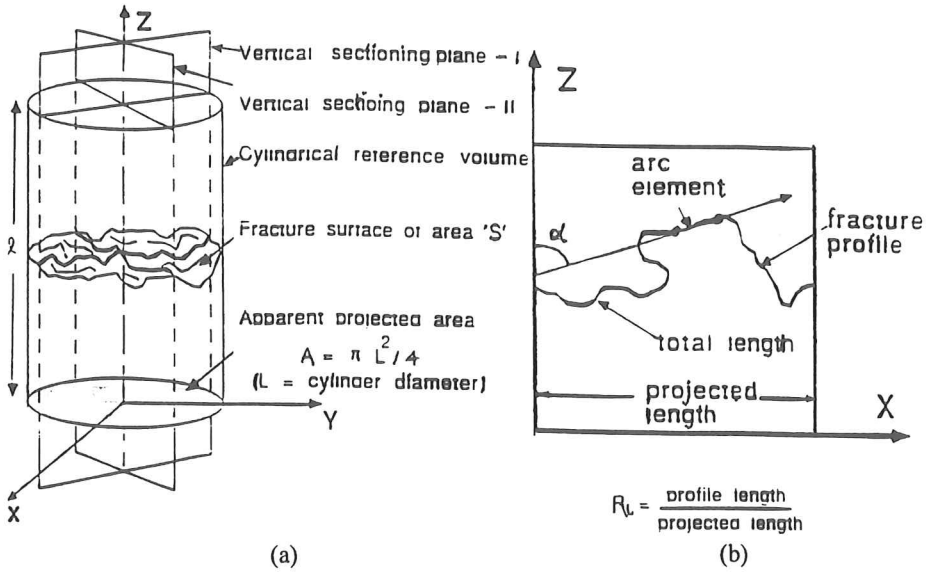


Fig. 8. (a) vertical sections of fracture surface, (b) profile orientation angle α

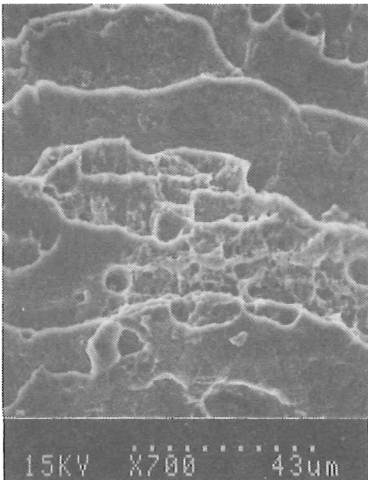


Fig. 9. SEM fractograph of the alloy 7050

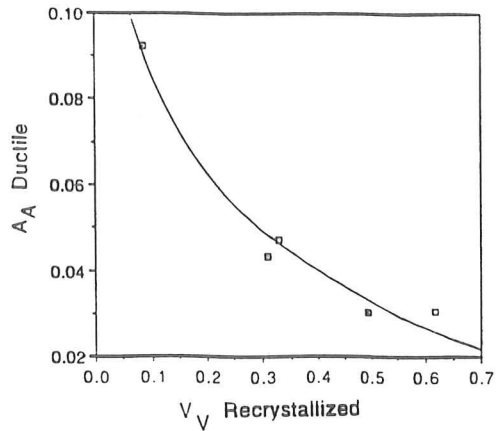


Fig. 10. Plot of V_V versus A_A ductile

on the fraction of the fracture surface area that is transgranular. The transgranular and intergranular regions of the fracture surface can be identified in SEM fractographs (see Figure 9). The presence and amount of recrystallized regions affects the fracture path and the fracture behavior of such materials (Staley, 1976). Thus, it is of interest to develop quantitative correlation between the volume fraction of the recrystallized regions in the alloy and the area fraction of transgranular fracture surface. A series of specimens of aluminum alloy 7050 having different amounts of recrystallized regions were prepared to study the correlation. Fracture surfaces were generated via standard tensile tests. Figure 9 shows a typical fracture surface produced in this manner. The values of area fraction of transgranular regions on the fracture surface were estimated by using point counting. The volume fraction of the recrystallized regions was estimated from a plane section through the bulk material. Figure 10 shows a plot of the area fraction of transgranular regions on the fracture surface versus the bulk volume fraction of the recrystallized regions in the material. There is a strong correlation between the fraction of the fracture path that is transgranular and the volume fraction of the recrystallized regions: the extent of transgranular fracture decreases with the increase in the volume fraction of recrystallized grains. Thus, the fracture behavior of the material can be controlled to a significant extent by controlling the amount of recrystallized grains in the alloy. This example demonstrates how simple stereological measurements such as point counting can yield quantitative information that is useful for alloy development.

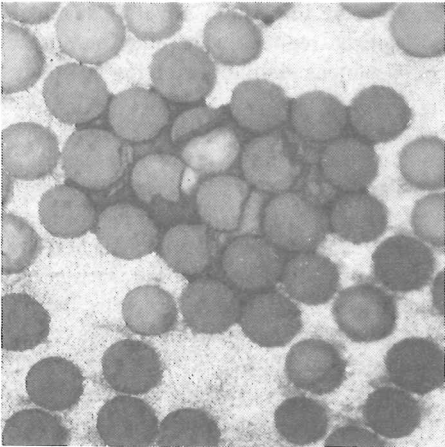
Processing Defects in Metal Matrix Composite

Metal matrix composites (MMC) often contain processing defects that may adversely affect their deformation and fracture behavior. Micrographs in Figure 11 show processing defects such as voids, oxide inclusions, segmented fibers, and oversized fibers in MMC having Al-Li alloy matrix and unidirectional continuous alumina fibers. In such a case it is of practical importance to know which defect(s) most adversely influence the failure processes, so that resources can be directed to decrease (or eliminate) such processing defects that most adversely affect the properties by controlling the process parameters. As shown in Figure 12 all the four processing defects are present on the fracture surface, and hence one can not draw any conclusions from qualitative observations. Stereological and quantitative fractographic measurements were performed to analyze this problem (Drury, 1989, Antolovich, et al., 1990). The number density and area fraction of the processing defects were measured on a series of tensile fracture surfaces generated from tensile tests performed on specimens having different orientations with respect to the tensile axis. The same measurements were performed on random metallographic planes through the bulk MMC. The data for processing voids and oxide inclusions (see Table I), reveal the following

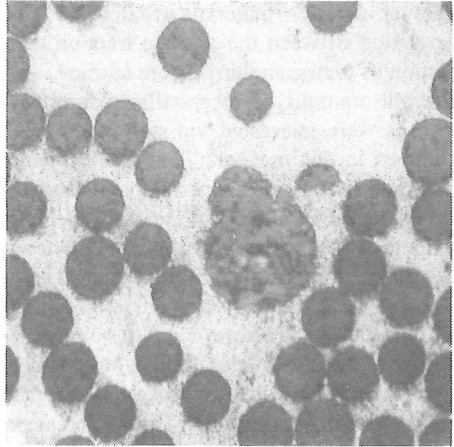
(1) In all the specimens, the number density and area fraction of processing void on fracture surface are significantly higher than their corresponding average values on random metallographic plane through bulk material. Thus, the fracture surface preferentially goes through the processing voids, and hence they are deleterious.

(2) The number density and area fraction of oxide inclusions on fracture surface are somewhat higher than their corresponding bulk values, but the differences are statistically significant only in some samples.

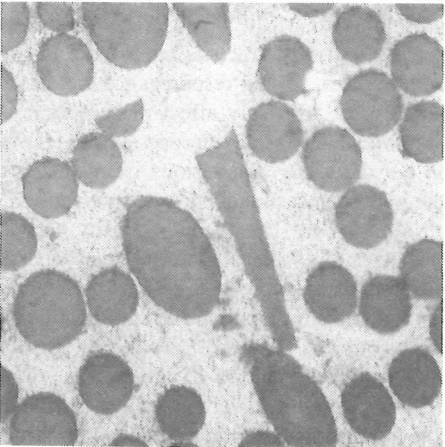
(3) The values of area fraction of oxide inclusions on fracture surfaces are comparable to those for the processing voids. However, the bulk values for area fraction of oxide inclusions are significantly higher than those for processing voids.



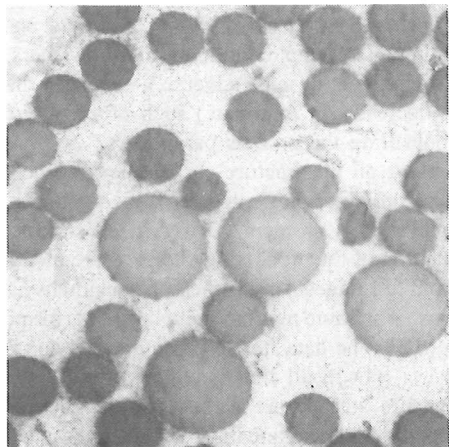
(a)



(b)

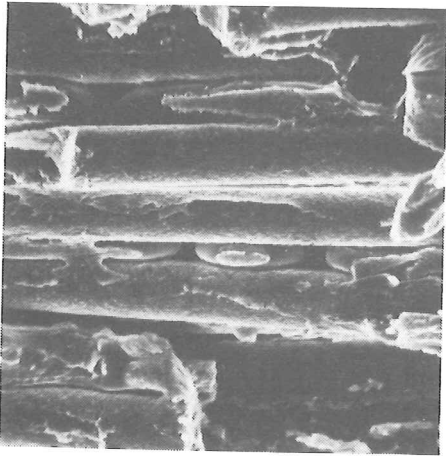


(c)

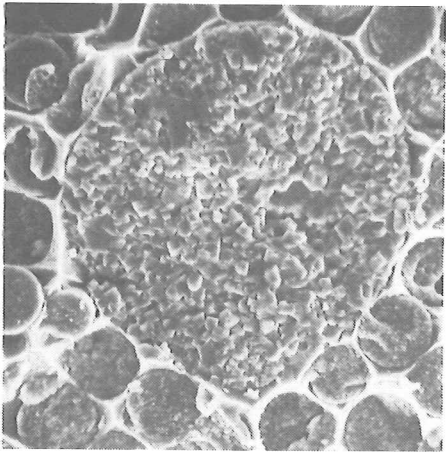


(d)

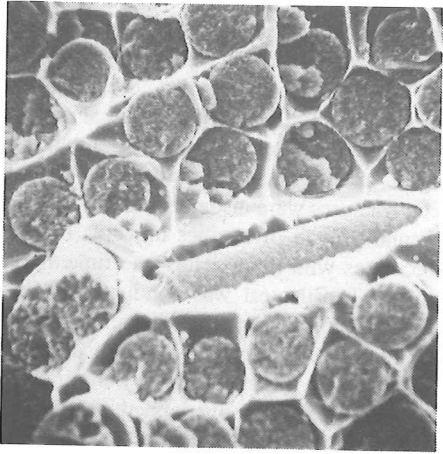
Fig. 11. Micrographs (at 500X) of processing defects in MMC such as: (a) processing voids, (b) oxide inclusions, (c) segmented fibers, and (d) oversized fibers in MMC.



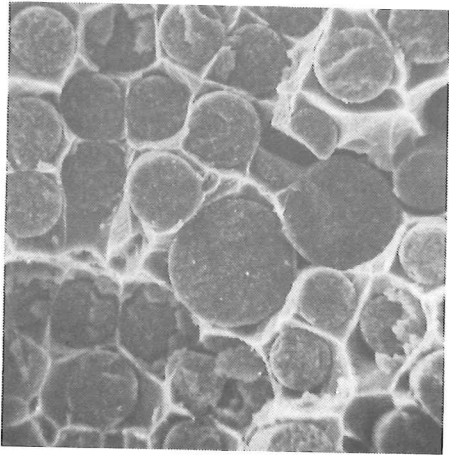
(a)



(b)



(c)



(d)

Fig. 12. SEM fractographs (at 500X) of processing defects in MMC such as: (a) processing voids, (b) oxide inclusions, (c) segmented fibers, and (d) oversized fibers in MMC.

Table 1. Values of area fraction, number density, and average area per defect on fracture surface and on a metallographic section through bulk.

Orientation	Area Fraction		Number Density, per mm ²		Average Area, μm ²	
	Voids	Oxide Particles	Voids	Oxide Particles	Voids	Oxide Particles
0°	0.0063 ^a	0.0050	11.3 ^a	4.0	560	1250
30°	0.0035 ^a	0.0040	8.2 ^a	4.8 ^a	430	830
60°	0.0104 ^a	0.0083 ^a	13.7 ^a	5.5 ^a	760 ^a	1510
90°	0.0118 ^a	0.0063 ^a	15.5 ^a	7.5 ^a	760 ^a	840
Bulk values	0.0004	0.0015	1.6	1.9	250	790

^a Statistically significant difference compared with the corresponding bulk parameter.

This example demonstrates that similar area fractions of the two types of defects on the fracture surface does not necessarily imply that they are equally important in the fracture processes; the appropriate conclusions can be drawn only after comparisons with the corresponding bulk values! In this particular case, the data indicates that the processing voids are more deleterious than the oxide inclusions.

Creep Fracture Surfaces

The components used for high temperature service may fail due to a number of different reasons such as creep, oxidation, tensile overload, etc. It is of interest to obtain information regarding the failure mode from examination of the fracture surface of failed component. Mishra (1992) and (Gokhale, Drury, Mishra, 1993) studied a number of creep and tensile fracture surfaces in order to pinpoint distinguishing topographic features of creep and tensile fractures. Interrupted creep tests were performed on OFHC copper at 400°C at different stress levels and for time periods ranging from 10% to 90% of creep life. Creep fractures were also generated at the same stress levels. The creep process leads to nucleation and growth of cavities or voids on grain boundaries. The volume fraction of these cavities increases with time. Thus interrupted creep test specimens contained varying amounts of cavities. Tensile test was conducted on each interrupted creep test specimen to generate tensile fracture surfaces from specimens having different volume fractions of cavities, (i.e., the fractures due to creep only). Vertical section fracture profiles were prepared from each fracture surface. The fracture profiles were digitized, and profile roughness parameter, fractal dimension, and fraction of overlapped profile were calculated from the profile data. It was observed that the roughness and fractal dimension increase with the amount of cavities. Creep fracture surfaces are rougher and more tortuous than the tensile fracture surfaces. However, the most important difference between the creep fracture and tensile fracture surfaces is the extent of overlaps on the fracture profile. Figure 13 shows a plot of the fraction of profile length having overlaps vs. cavity volume fraction for tensile and creep fracture surfaces. It is interesting to note that creep fracture surfaces have significantly higher (more than factor of two) overlaps than the tensile fracture surfaces, even for the same cavity volume fraction.

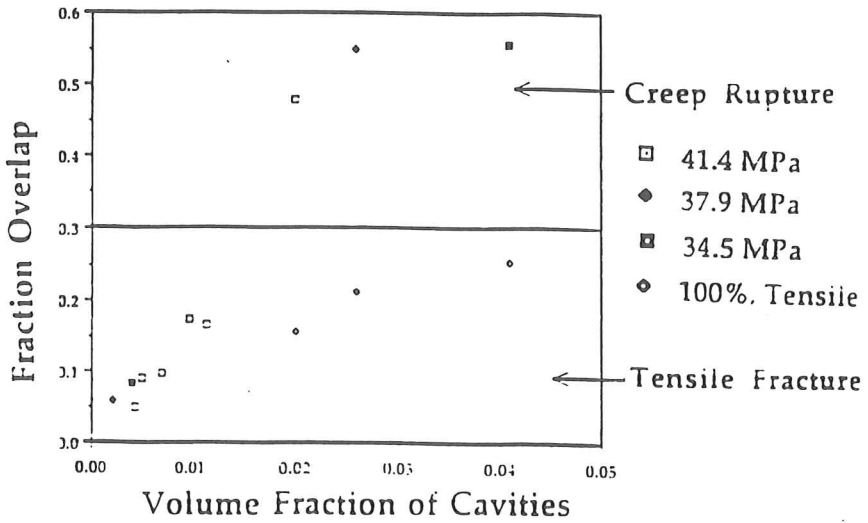
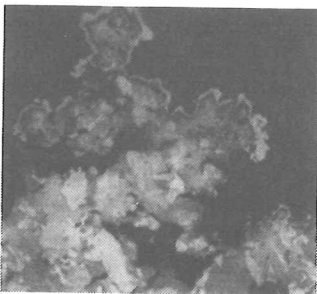
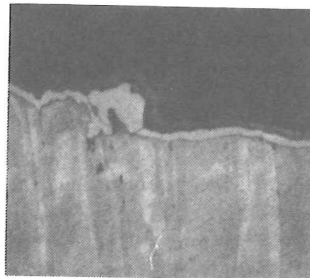


Fig. 13. Fraction of overlapping profile versus V_v of cavities in copper.

A large amount of overlaps appear to be a distinguishing feature of the creep fracture surfaces! This observation should be useful for failure analysis of components in high temperature service. This can be seen from Figure 14.



100X
(a)



200X
(b)

Fig. 14. Micrographs showing fracture profiles of (a) creep, (b) tensile fracture of copper

SUMMARY

Some practical applications of stereology in the study of materials are presented. It is shown that even simple measurements such as point counting and line intersection counting can give useful information concerning materials processes. The measurements on fracture surfaces give important insights into the failure processes and the role of microstructure in deformation and fracture of materials.

ACKNOWLEDGEMENT

This work was supported by research grants from the National Science Foundation (DMR - 9013098 and 9301986) and the Aluminum Company of America. The financial support is gratefully acknowledged.

REFERENCES

- Antolovich SD, Gokhale AM, Bathias C. Application of quantitative fractography and computed tomography to fracture processes in materials. ASTM Special Tech Pub No. 1085. 1990; 1085 : 3-25.
- Banerji K. Quantitative fractography: a modern perspective. Metall Trans 1988; 19A: 264-271.
- Baddeley AJ, Gundersen HJG, Cruz-Orive LM. Estimation of surface area from vertical sections. J Microsc 1986; 142: 259-276.
- Cruz-Orive LM. Particle number can be estimated using disector of unknown thickness: the selector. J Microsc 1987; 145: 121-142.
- Cruz-Orive LM. Second order stereology: estimation of second moment volume measures. Acta Stereol 1989; 8, Suppl. II: 641-646.
- Cruz-Orive LM, Howard CV. Estimating the length of bonded curve in three dimensions using total vertical projections. J Microsc 1991; 163: 101-113.
- DeHoff RT. Microstructural evolution during recrystallization. In: Hansen N, Jensen DJ. eds. Annealing processes: recovery, recrystallization and grain growth. Denmark: Riso, Roskilde, 1986: 35-52.
- DeHoff RT. Use of the disector to estimate the Euler characteristic of three dimensional microstructures. Acta Stereol 1987; 6: 133-140.
- Drury WJ. Role of processing defects in fracture of a metal matrix composite. Metall Trans 1989; 20A: 2175-2178.
- Drury WJ. Ph.D. thesis. Development of quantitative fractography and its application to the study of fracture processes of materials. Georgia Institute of Technology, Atlanta 1992.
- Drury WJ, Gokhale AM. Measurement and interpretation of fracture surface fractal dimension. ASTM Special Tech Pub No. 1165, 1993; 1165: 295-310.
- Gokhale AM. Unbiased estimation of curve length in 3D using vertical slices. J Microsc 1990; 159: 133-141.
- Gokhale AM. Estimation of length density from vertical slices of unknown thickness. J Microsc 1992; 167: 1-8.
- Gokhale AM. Utility of horizontal slice for stereological characterization of lineal features. J Microsc 1993; 170: 3-8.
- Gokhale AM. Evolution of bivariate particle size distributions. Metall Trans 1992; 23A: 2973-2980.

- Gokhale AM, DeHoff RT. Estimation of nucleation rate and growth rate from time dependence of global microstructural properties. *Metall Trans* 1985; 16A: 359-364.
- Gokhale AM, Basavaiha M, Upadhyaya GS. Kinetics of neck growth during loose stack sintering. *Metall Trans* 1988; 19A: 2153-2161.
- Gokhale AM, Underwood EE. A general method for estimation of fracture surface roughness; part - I theoretical aspects. *Metall Trans* 1990; 21A: 1193-1199.
- Gokhale AM, Drury WJ. A general method for estimation of fracture surface roughness; part - II practical considerations. *Metall Trans* 1990; 21A: 1201-1207.
- Gokhale AM, Drury WJ. Surface roughness of anisotropic fracture surfaces. *Materials Characterization* 1993; 30: 279-286.
- Gokhale AM, Whited WT. Measurements of growth rate of thermally induced microcracks in a metal matrix composite. In: Upadhyaya K. ed. *Proceedings of symposium on: Developments in Ceramic and Metal Matrix Composites*. ASM 1992: 273-286.
- Gokhale AM, Drury WJ, Mishra S. Recent developments in quantitative fractography. *ASTM Special Technical Publication* 1993; 1203: 3-22.
- Gundersen HJG. The nucleator. *J Microsc* 1988; 151: 3-21.
- Jensen EB, Kieu K, Gundersen HJG. Second order stereology. *Acta Stereol* 1990; 9: 15-35.
- McMillan PJ. Areal analysis revisited: precision of the ribbon probe. *Acta Stereol* 1992; 11/Suppl 1: 387-390.
- Mandelbrot BB. *Fractal geometry of nature*. New York: W.H. Freeman and Co., 1983.
- Meyer F. *Mathematical morphology: from two dimensions to three dimensions*. *J Microsc* 1992; 165: 5-28.
- Mishra S. M.S. thesis. *Stereological assessment of the evolution of microstructural damage during creep*. Georgia Institute of Technology, Atlanta 1991.
- Serra J. *Image analysis and mathematical morphology*. Theoretical advances: Vol. 2. London: Academic press, 1988.
- Staley JT. *Microstructure and toughness of high-strength aluminum alloys*. *ASTM Special Technical Publication* 1976; 605: 71-103
- Sterio DC. The unbiased estimation of number and sizes of arbitrary particles using dissector. *J Microsc* 1984; 134: 127-136.
- Stoyan D. *Stereological determination of orientation, second order quantities and correlations for random fiber systems*. *Biom J*. 1985; 27: 411-425.
- Underwood EE. *Quantitative Stereology*. Reading, Mass.: Addison-Weseley, 1970
- Vandermeer RA. *Modelling of microstructural evolution*. *Scripta Met Mater* 1992; 27:1563-1568.
- Whited WT. M.S. thesis. *Microstructural damage evolution during thermal cycling of metal matrix composites*. Georgia Institute of Technology, Atlanta 1992.